RSC Advances

This is an *Accepted Manuscript*, which has been through the Royal Society of Chemistry peer review process and has been accepted for publication.

Accepted Manuscripts are published online shortly after acceptance, before technical editing, formatting and proof reading. Using this free service, authors can make their results available to the community, in citable form, before we publish the edited article. This *Accepted Manuscript* will be replaced by the edited, formatted and paginated article as soon as this is available.

You can find more information about *Accepted Manuscripts* in the Information for Authors.

Please note that technical editing may introduce minor changes to the text and/or graphics, which may alter content. The journal's standard Terms & Conditions and the Ethical guidelines still apply. In no event shall the Royal Society of Chemistry be held responsible for any errors or omissions in this *Accepted Manuscript* or any consequences arising from the use of any information it contains.

ROYAL SOCIETY OF CHEMISTRY

www.rsc.org/advances

Fe_2O_3-AgBr Nonwoven Cloth with Hierarchical Nanostructures as Efficient and Easily Recyclable Macroscale Photocatalysts [1]

Huihui Zhao,[a] Lisha Zhang,*[a] Xiaodong Gu,[b] Shijie Li,[a] Bo Li,[b] Huanli Wang,[a] Jianmao Yang,[c] Jianshe Liu*[a]

ABSTRACT

A prerequisite for the development of photocatalytic application is to obtain efficient and easily recycled visible-light-driven (VLD) photocatalysts. Usually, nanosized photocatalysts exhibit excellent photocatalytic performances but can not be easily recycled, and film-shaped nanostructured photocatalysts on the substrates (or magnetic photocatalysts) can be easily recycled but have low surface area and/or high production cost. To solve this problem, herein we report on the design and preparation of nonwoven cloth based on semiconductor-semiconductor (Fe_2O_3-AgBr as the model) nanojunctions as efficient and easily recyclable macroscale photocatalysts with nanostructure. Fe_2O_3-AgBr nonwoven cloth has been prepared by a simple electrospinning-calcination method. Such macroscale cloth is free-standing and it consists of hierarchical pores with diameters of 600-750 nm and nanofibers with diameters of 150-350 nm. Furthermore, these nanofibers are constructed from Fe_2O_3 and AgBr nanoparticles with diameters of ~ 60 nm. In addition, Fe_2O_3-AgBr nonwoven cloth has magnetic property and the broadened visible-light photo-response range (400 ~ 750 nm). Under the irradiation of visible light, Fe_2O_3-AgBr nonwoven cloth exhibits higher photocatalytic activity than Fe_2O_3 nonwoven cloth and AgBr nonwoven cloth containing the

* Corresponding authors. Tel.: +86-21-67792523; fax: +86-21-67792522.
E-mail address: lszhang@dhu.edu.cn (L.S. Zhang); liujianshe@dhu.edu.cn (J.S. Liu).

RSC Advances Accepted Manuscript

same weight of visible-light-active component, for the degradation of rhodamine B (RhB) and parachlorophenol (4-CP). Higher photocatalytic activity of Fe_2O_3-AgBr nonwoven cloth should result from the synergic effects between Fe_2O_3 and AgBr due to the broadening photoabsorption and the energy level matching. Importantly, Fe_2O_3-AgBr nonwoven cloth can be easily transferred and/or recycled by diping/pulling method and/or external magnetic field, and it has excellent photocatalytic stability during recycling test. Therefore, this work provides some insight into the design and development of novel, efficient and easily recyclable macroscale nonwoven cloths, for future practical photocatalytic application, for example, degrading organic pollutants in the polluted river.

1. Introduction

Over the past years, semiconductor photocatalysis has drawn much attention as a potential solution to the worldwide energy shortage and environmental purification. [1] A prerequisite for the development of photocatalysis application is to obtain photocatalysts. To date, TiO_2 is undoubtedly one of the most excellent and widely used photocatalysts due to its abundance, chemical stability, low cost, and nontoxicity.[2,3] But a major drawback of TiO_2 is its large bandgap (~ 3.2 eV) and thus only UV light (typically $\lambda < 400$ nm; a small fraction of solar spectrum, ~ 5 %) can be absorbed, which significantly limits the utilization of solar light in the visible region ($400 < \lambda < 700$ nm).[2,3] To address this problem, the development of visible-light-driven (VLD) photocatalysts has attracted increasing attention. Up to now, a series of single-component semiconductor nanomaterials have been developed as VLD photocatalysts, such as simple metal oxides (Cu_2O,[4] $W_{18}O_{49}$,[5] Bi_2O_3,[6] and etc.), complex oxides (Bi_2WO_6,[7,8] BiOCl,[9] $ZnGa_2O_4$,[10] Ag_3PO_4,[11] and etc.), metal sulfides (CdS,[12] $ZnIn_2S_4$,[13]

RSC Advances Accepted Manuscript

and etc.) and other non-metal materials (g-C_3N_4[14]). We have also developed some simple/complex oxides, such as Bi_2O_3[15] and Bi_2WO_6 superstructures[7,8] as VLD photocatalysts. However, there are still some drawbacks hindering their practical application, including the unsatisfactory visible-light photoresponse range, short photogenerated electron-hole pair lifetimes, and recycle difficulty. To meet the requirements of future environmental and energy technologies, it is still necessary to further develop efficient and easily recycled VLD photocatalysts.

On one hand, to improve the photocatalytic activity of VLD photocatalysts, a variety of strategies have been employed, for example, via suitable textural design, doping, and forming a semiconductor heterojunction by combining them with metal and/or other semiconductors[16]. Among these methods, the construction of semiconductor heterojunctions has attracted much attention due to its simplicity and effectiveness. Recently, we have summarized the design principles and fabrication methods of semiconductor heterojunction nanomaterials as efficiently VLD photocatalysts[16], including the semiconductor-semiconductor heterojunction (such as WO_3-$BiVO_4$[17], C_3N_4-MoS_2[18], Bi_2O_3-Bi_2WO_6[19] and $BiVO_4$-FeOOH-NiOOH[20]), the semiconductor-metal heterojunction (such as Bi_2WO_6-Ag[21], AgCl-Ag[22] and Ag_3PO_4-Ag[23]), the semiconductor-carbon heterojunction (such as Cu_2O-carbon nanotubes[24] and CdS-graphene[25]) and the multicomponent heterojunction (such as, CdS-Au-TiO_2[26], and AgBr-Ag-Bi_2WO_6[27,28]). Compared with single-component semiconductor, these semiconductor heterojunction nanomaterials exhibit high photocatalytic activity for the degradation of organic pollutants, hydrogen generation, and/or photocatalytic disinfection.[17-28] Unfortunately, it is usually difficult to recycle these nanosized photocatalysts in practical application (such as degrading organic pollutants in lake and/or river), resulting in

RSC Advances Accepted Manuscript

second-contamination and limiting their large scale application.

On the other hand, to effectively recycle catalyst, two strategies have been chiefly developed. The first kind is to prepare nanostructured semiconductor films on the substrates, such as nanoparticles-based composite films on ITO glass,[29,30] nanowires/nanotubes-based film grew on metal foil.[31,32] These film-shaped photocatalysts on the substrate can be easily recycled, but they suffer from the problems, such as relatively low surface area and/ or high production cost. The second kind is to prepare nano-photocatalysts with magnetic component, such as pure Fe_2O_3,[33,34] Fe_2O_3-Bi_2WO_6,[35] Ag-AgI/Fe_3O_4@SiO_2 (X= Cl, Br, or I),[36] etc. These magnetic nanocomposites as photocatalysts can be easily recycled by external magnetic field in the laboratory, but it is still inconvenient to recycle them in practical application (such as degrading organic pollutants in lake and/or river). In addition, the photocatalytic performances of these photocatalysts are still unsatisfied in practical application.

Thus, the development of efficient and easily recycled VLD photocatalysts remains a great challenge. To solve this issue, recently we have deduced that macroscale semiconductor photocatalysts with nanostructure may have great potential as new generation photocatalysts that have simultaneously a broad range of visible-light response, superior photocatalytic activity, high photostability, low cost and easily recycling characteristics, etc.[37] With Ta_3N_5 as a model semiconductor, we prepared Ta_3N_5-Pt nonwoven cloth with hierarchical nanopores by an electrospinning-calcination-nitridation-wet impregnation method.[37] Ta_3N_5-Pt nonwoven cloth can be used as an efficient and easily recyclable macroscale photocatalyst with wide visible-light response. However, this is just a preliminary attempt to develop nonwoven cloth based on semiconductor-metal heterojunction. A lot of work should be done to further improve the performance of photocatalyst, for example, by preparing and optimizing

RSC Advances Accepted Manuscript

nonwoven cloth based on semiconductor-semiconductor and semiconductor-carbon heterojunction.

Among semiconductor photocatalysts, Fe_2O_3 nanomaterials with band gap of 2.0 ~ 2.2 eV have magnetic properties and can utilize a large fraction of visible light, thus they have been considered to be magnetic and efficient VLD photocatalysts.[33,34] In addition, AgBr with band gap of 2.6 eV has also been proved to be an excellent VLD photocatalyst.[38,39] Herein, by using Fe_2O_3 and AgBr as the models of semiconductors, we report the design and preparation of nonwoven cloth based on semiconductor-semiconductor (Fe_2O_3-AgBr) nanojunctions. Macroscale Fe_2O_3-AgBr nonwoven cloth consists of plenty of nanofibers, and these nanofibers are in fact constructed from Fe_2O_3 and AgBr nanoparticles. The Fe_2O_3-AgBr nonwoven cloth can be used as an efficient macroscale semiconductor heterojunction photocatalyst with nanostructure, for the degradation of both rhodamine B (RhB) dye and parachlorophenol (4-CP) under visible-light irradiation. Importantly, Fe_2O_3-AgBr nonwoven cloth can be easily recycled with good stability, by diping/pulling method and/or external magnetic field.

2. Experimental

2.1. Materials

Ferric acetylacetonate ($Fe(acac)_3$), polyvinyl pyrrolidone (PVP, $M_W \approx 1300000$), cetyltrimethylammonium bromide (CTAB), silver nitrate, ammonium hydroxide (25 wt% NH_3), ethanol (> 99.7 %) and acetic acid were purchased from Sinopharm Chemical Reagent Co., Ltd. They were all analytical grade and used as received without further purification.

2.2. Preparation of catalysts

RSC Advances Accepted Manuscript

Fe_2O_3-AgBr nonwoven cloth was synthesized by an electrospinning-calcination method. In a typical process, $Fe(acac)_3$ (0.65 g, 1.84 mmol), PVP (1.5 g) and CTAB (0.35 g, 0.96 mmol) were dissolved in ethanol (16 mL). Then the ethanol solution was magnetically stirred for 30 min, forming a turbid solution. Subsequently, ammonia water (1 mL) containing $AgNO_3$ (0.10 g, 0.59 mmol) was quickly added to the above solution. After vigorously stirring for 24 h, the precursor solution was loaded into a plastic syringe, and the feeding rate was kept constant at 0.5 mL h^{-1} using a syringe pump. A high voltage of 16 kV was applied between the orifice and grounded aluminum foil at a distance of 15 cm. The collected composite cloth was taken out carefully, hydrolyzed in air for 12 h, and calcined at 550℃ in air for 6 h to obtain Fe_2O_3-AgBr nonwoven cloth.

For comparison, Fe_2O_3 nonwoven cloth as well as AgBr nonwoven cloth was also synthesized by an electrospinning-calcination method. The precursor solution for Fe_2O_3 nonwoven cloth was the ethanol solution (16 mL) containing 2.08 g $Fe(acac)_3$, 1.12 g PVP and 4.8 mL acetic acid. Then the electrospinning process was performed under the same conditions with the preparation of Fe_2O_3-AgBr nonwoven cloth. The precursor solution for AgBr nonwoven cloth was the ethanol solution (16 mL) containing 0.35 g CTAB, 1.5 g PVP, 0.10 g $AgNO_3$ and 1 mL ammonia water; and the electrospinning-calcination process was the same with those of Fe_2O_3-AgBr nonwoven cloth.

2.3. Photocatalysts characterization

The sizes and morphologies of samples were examined by field emission scanning electron microscope (FE-SEM, Hitachi S-4800) and high-resolution transmission electron microscope (HR-TEM, JEOL JEM-2010F). X-Ray diffraction (XRD) was measured with a D/max-2550 PC X-ray diffractometers using Cu-Kα radiation (λ = 0.15418 nm).

RSC Advances Accepted Manuscript

Energy-dispersive X-ray spectroscopy (EDS) of the sample was carried out on a Bruker Quantax 400 EDS system during SEM characterization. The optical diffuse reflectance spectra of the samples were measured on a UV-VIS-NIR scanning spectrophotometer (UV-3101PC, Shimadzu) using an integrating sphere accessory. Magnetic properties were measured with a physical property measurement system (PPMS-9T (EC-II)).

2.4. Photocatalytic test and reusability of nonwoven cloth

Photocatalytic activities of the photocatalysts were tested by degrading rhodamine B (RhB) and parachlorophenol (4-CP), using a 300 W xenon lamp (Beijing Perfect Light Co. Ltd., Beijing) as light source. Light was passed through a UV cut-off filter (λ> 400 nm), and then was focused onto a 100-mL beaker containing aqueous solution of RhB (40 mL, 4.79 mg L^{-1}, pH = 7.0) or 4-CP (50 mL, 10 mg L^{-1}). The temperature of the reaction solution was controlled at 20 ± 2°C by circulation cooling installation. In each experiment, a feasible amount of photocatalysts were added into aqueous solution. Prior to irradiation, the suspensions were magnetically stirred for 60 min in the dark to achieve adsorption-desorption equilibrium between the photocatalyst and the target organic pollutant.

When the remaining RhB concentration needed to be measured, at 10 min irradiation time intervals, 1.5 mL aliquot was collected, centrifuged, and then filtered through a Millipore filter (pore size 0.22 μm) to remove the catalysts for analysis. The filtrate was analyzed by recording variations at the wavelength of maximal absorption (553 nm) in the UV-vis spectra of RhB with a U-2910 (Hitachi, Japan) spectrophotometer. Meanwhile, to study the pH effect on the photocatalytic activity, the initial pH of RhB aqueous solution was tuned to be 3, 5, 7, 9, or 11 by adding H_2SO_4 (0.1 mol L^{-1}) or NaOH (0.1 mol L^{-1}) aqueous solution, and the degradation efficiency of RhB by Fe_2O_3-AgBr nanowoven cloth was measured.

RSC Advances Accepted Manuscript

When the remaining 4-CP concentration needed to be measured, at 20 min irradiation time intervals, 5 mL aliquot was collected, centrifuged, and then filtered to be analyzed. The 4-CP concentrations in the solutions were analyzed by high-performance liquid chromatography (HPLC) using an Agilent 1100 series (USA) equipped with a diode array detector (DAD). The mobile phase consisted of 80 % acetonitrile and 20 % water at a flow rate of 0.5 mL min^{-1}. The maximum absorption wavelength was detected at 280 nm.

To test the mineralization degree of 4-CP, the photodegradation by Fe_2O_3-AgBr nanowoven cloth was performed under visible-light irradiation. 300 mg Fe_2O_3-AgBr nonwoven cloth was immersed to 100 mL 4-CP solution (20 mg L^{-1}). During the photocatalytic process, at 30 min irradiation time intervals, 10 mL aliquot was collected, centrifuged, and then filtered through a Millipore filter (pore size 0.22 μm) to remove the catalyst particulates for analysis. The total organic carbon (TOC) value of 4-CP was detected by a Shimadzu TOC-V_{CPH} total organic carbon analyzer.

To test the stability and reusability of Fe_2O_3-AgBr nanowoven cloth, four consecutive cycles of photodegrade RhB were proceed under visible-light irradiation. After one cycle photocatalytic reaction, the photocatalysts were recycled by diping/pulling method (2 times) or external magnetic field (1 time). Then, the collected photocatalysts were washed thoroughly with water and dried at 75 °C for 12 h. Next, the dried Fe_2O_3-AgBr nanowoven cloth was immersed to photodegrade fresh RhB aqueous solution (40 mL, 4.79 mg L^{-1}) again.

3. Results and discussion

3.1. Preparation and characterization of the nonwoven cloth

Fe_2O_3-AgBr nonwoven cloth was prepared by an electrospinning-calcination method, as

RSC Advances Accepted Manuscript

demonstrated in Fig. 1. First step was to prepare PVP/Fe_2O_3-AgBr/CTAB composite nonwoven cloth, by electrospinning the ethanol solution (16 mL) containing 0.65 g $Fe(acac)_3$, 0.35 g CTAB, 1.5 g PVP, 0.10 g $AgNO_3$ and 1 mL ammonia water at a high voltage of 16 kV, and followed by the hydrolysis process. The as-prepared PVP/Fe_2O_3-AgBr/CTAB composite nonwoven cloth is yellow, and its typical photograph (area: ~ 6 × 4 cm^2) is shown in Fig. 2a. In fact, in the electrospinning process, the area of the nonwoven cloth can be easily tuned in a broad range (10^{-4} ~ 1 m^2) by changing the collecting region of aluminum foil. This macroscale nonwoven cloth is composed of plenty of individual straight fibers with smooth surface and diameters ranging from 350 to 400 nm, as revealed in SEM images (Fig. 2b and 2c). In addition, among fibers in the nonwoven cloth, there are many hierarchical pores with diameter of 600-750 nm (Fig. 2b and 2c).

The second step was to calcine the composite nonwoven cloth at 550 °C in air for 6 h, for removing organic component and obtaining inorganic Fe_2O_3-AgBr nonwoven cloth. It should be noted that the area of Fe_2O_3-AgBr nonwoven cloth was reduced to ~ 1 × 1.5 cm^2, since nonwoven cloth with larger area may be more fragmented. After the calcination process, the color of the nonwoven cloth turned from yellow to red-brown, as demonstrated vividly in Fig. 2d. This Fe_2O_3-AgBr nonwoven cloth has the macroscopic morphology and is still freestanding (Fig. 2d), indicating that the calcination process has no obvious adverse effect on the macroscopic morphology. SEM images (Fig. 2e and 2f) reveal that Fe_2O_3-AgBr cloth is also composed of hierarchical pores (diameter: 600-750 nm) and fibers. The diameters of Fe_2O_3-AgBr fibers shrink to 150-350 nm, and these fibers also interweave and/or stick together, which results from the decomposition of PVP/CTAB component and high temperature anneal of Fe_2O_3-AgBr component. Further information about Fe_2O_3-AgBr

RSC Advances Accepted Manuscript

206 nanofiber is obtained from the TEM image (Fig. 2g), and it confirms that the Fe_2O_3-AgBr
207 nanofiber with diameter of about 200 nm is comprised of plenty of nanoparticles with
208 diameters of ~ 60 nm, probably resulting in high surface area. The high-resolution TEM
209 image (Fig. 2h) taken from one nanoparticle in the fiber (Fig. 2g) demonstrates that the lattice
210 spacings are 0.271 and 0.333 nm, which are in good agreement with the values for the Fe_2O_3
211 (104) plane (JCPDS Card. 87-1166) and for the AgBr (111) plane (JCPDS Card. 79-0149),
212 respectively. Thus, one can confirm the formation of Fe_2O_3-AgBr nonwoven cloth with
213 well-defined nanojunctions.

214 Subsequently, the phase and composition of Fe_2O_3-AgBr nonwoven cloth were further
215 investigated. Fig. 3a shows the XRD pattern of Fe_2O_3-AgBr nonwoven cloth as well as the
216 standard XRD patterns of AgBr (JCPDS Card. 79-0149) and Fe_2O_3 (JCPDS Card. 87-1166).
217 Obviously, XRD pattern of Fe_2O_3-AgBr nonwoven cloth can be indexed as the mixture of
218 Fe_2O_3 crystalline and AgBr crystalline. Some diffraction peaks at 30.94° , 44.33° and 55.04°
219 are assigned to (200), (220) and (222) crystal planes of cubic phase AgBr (JCPDS Card.
220 79-0149), respectively. In addition, some diffraction peaks at 24.15°, 33.3°, 35.8°, 41.0°,
221 49.6°, 54.8°, 62.6°, 64.2° are corresponding to (012), (104), (110), (113), (024), (116), (214)
222 and (300) crystal planes of rhombohedral Fe_2O_3 (JCPDS Card. 87-1166), respectively. These
223 results confirm that there are both Fe_2O_3 and AgBr species in the
224 semiconductor-semiconductor nanojunction system, which is in good agreement with the
225 HR-TEM analysis (Fig. 2h). In addition, since Fe_2O_3-AgBr nonwoven cloth was prepared by
226 electrospinning-calcination process without washing/centrifugation step, $Fe(acac)_3$ (1.84
227 mmol) and $AgNO_3$ (0.59 mmol) should be converted completely to Fe_2O_3 and AgBr species
228 without Fe/Ag element loss. The resulting Fe_2O_3-AgBr nonwoven cloth was about 0.26 g, and

RSC Advances Accepted Manuscript

it should consist of 0.92 mmol (~ 0.147 g, 57 wt %) Fe_2O_3 and 0.59 mmol (~ 0.111 g, 43 wt %) AgBr with Fe/Ag molar ratio of about 3.1. EDS pattern (Fig. 3b) further reveals that there are O, Fe, Br and Ag elements in the Fe_2O_3-AgBr nonwoven cloth, and the molar ratio of Fe to Ag is equal to 2.9 which is close to the precursor Fe/Ag molar ratio (3.1). Therefore, one can deduce that Fe_2O_3-AgBr nonwoven cloth was composed of Fe_2O_3 (57 wt %) and AgBr (43 wt %) crystallines.

The magnetic property of Fe_2O_3-AgBr nonwoven cloth was measured at 300 K with the magnetic field swept back and forth between 30 and -30 kOe. Fig. 4a shows a nonlinear and reversible behavior with a magnetic hysteresis loop. And a detailed partial image is shown in the inset of Fig. 4a. The relevant saturation magnetization (M_s), remanent magnetization (Mr) and coercivity (Hc) of Fe_2O_3-AgBr nonwoven cloth were 8.42 emu/g, 1.2 emu/g and 160 G respectively, revealing super paramagnetic behavior. Magnetic characteristic provides a promising way for catalyst recycling because it not only prevents the loss of catalyst but also saves time. In our case, the Fe_2O_3-AgBr nonwoven cloth could be precipitated in the water (Fig. 4b), but it could be magnetically pulled to the side of the bottle when an external column magnet was applied on the same side of the bottle (Fig. 4c). These facts reveal that Fe_2O_3-AgBr nonwoven cloth can be efficiently recycled by external magnetic field.

The optical absorption of Fe_2O_3-AgBr nonwoven cloth was measured by an UV-vis spectrometer (Fig. 5). For comparison, the optical absorption of Fe_2O_3 nonwoven cloth prepared by electrospinning-calcination was also tested. Fe_2O_3 nonwoven cloth exhibits photoabsorption from the UV to visible light with edge at approximately 610 nm, which agrees well with the reported value for the band gap (Eg = 2.0 eV) of bulk Fe_2O_3.[33] The weak absorption from 610 nm to 750 nm is occurred, which should result from the effective light

RSC Advances Accepted Manuscript

scattering. Importantly, Fe_2O_3-AgBr nonwoven cloth displays a broader-spectrum photoabsorption from the UV light to visible light region with edge at approximately 630 nm and the weak absorption from 630 nm to 750 nm, indicating a substantial red shift of photoabsorption. Furthermore, the photoabsorption of Fe_2O_3-AgBr nonwoven cloth in the whole visible light region (400 nm ~ 750 nm) is higher than that of Fe_2O_3 nonwoven cloth. These facts demonstrate that the region of visible-light photo-response of Fe_2O_3-AgBr nonwoven cloth can be broadened and enhanced due to the construction of the heterojunction. Therefore, VLD photocatalytic activity of Fe_2O_3-AgBr nonwoven cloth can be expected to be more excellent compared with that of pure Fe_2O_3 nonwoven cloth.

3.2 Photocatalytic performances of Fe_2O_3-AgBr nonwoven cloth

In order to investigate the potential of Fe_2O_3-AgBr nonwoven cloth as VLD photocatalyst, the photocatalytic activity of macroscopic Fe_2O_3-AgBr cloth was evaluated by immersing the cloth in the solution containing RhB dye or 4-CP as the model pollutant (Fig. 6a). For comparison, Fe_2O_3 and AgBr nonwoven cloths were also prepared and used as the photocatalysts.

When RhB dye was used as the model of colored organic pollutant, the photocatalytic degradation efficiency by macroscopic Fe_2O_3-AgBr nonwoven cloth (20 mg, containing 11.4 mg Fe_2O_3 and 8.6 mg AgBr) was evaluated under visible light irradiation (λ> 400 nm) (Fig. 7a). For comparison, the degradation efficiencies of RhB dye without photocatalysts (blank test) and by different photocatalysts with the same weight of each component (11.4 mg pure Fe_2O_3 nonwoven cloth, or 8.6 mg pure AgBr nonwoven cloth) were determined with otherwise identical conditions, respectively, as shown in Fig. 7a. The blank test indicates that the degradation of RhB is extremely slow without photocatalysts under visible light

RSC Advances Accepted Manuscript

illumination (Fig. 7a-A). When the pure Fe_2O_3 nonwoven cloth (11.4 mg) was used as the photocatalyst, the degradation of RhB was also slow, and only 13.7 % RhB could be removed after 60 min of reaction (Fig. 7a-B). By using the pure AgBr nonwoven cloth (8.6 mg) as the photocatalyst, 25.9 % of RhB was photocatalytically degraded after 60 min, indicating low photocatalytic activity (Fig. 7a-C). Importantly, when Fe_2O_3-AgBr cloth was used as the photocatalyst, 91.8 % of RhB could be degraded after 60 min, indicating the highest photocatalytic activity, as shown in Fig. 7a-D.

Subsequently, the effect of pH value of solutions on photodegradation efficiency of RhB was studied by using Fe_2O_3-AgBr nonwoven cloth (20 mg) as the photocatalyst, and the degradation efficiency at 60 min was determined (Fig. 7b). Obviously, when the pH was acid or alkaline, the photodegradation efficiency was relatively slow (66.5 % at pH = 3 or 70.7 % at pH = 11). However, the photodegradation efficiency of RhB enhanced when the RhB aqueous solution was close to neutral condition (75.3 % at pH = 5 or 76.0 % at pH = 9). Especially, when the pH value was 7.0, 91.8 % RhB could be photodegraded after 60 min. Previous studies reveal that the photodegradation of dye pollutants is pH-dependent, chiefly resulting from the variation of surface charge of catalysts and the structure of the dye molecule with pH.[27] We also believe that the variation of degradation efficiency of RhB should be attributed to surface charge of catalysts and the structure of the dye molecule.

When 4-CP was used as the model of colorless organic pollutant, the photocatalytic degradation efficiencies were evaluated by blank test (without photocatalysts) or immersing pure Fe_2O_3 nonwoven cloth (28.5 mg), pure AgBr nonwoven cloth (21.5 mg), or Fe_2O_3-AgBr nonwoven cloth (50 mg, containing 28.5 mg Fe_2O_3 and 21.5 mg AgBr) in 4-CP aqueous solution under visible light irradiation ($\lambda > 400$ nm) (Fig. 8a). 4-CP as a typical pollutant has

RSC Advances Accepted Manuscript

no photolysis and no visible light absorption characteristics in the photodegradation process. The blank test reveals that there was no photodegradation of 4-CP after 120 min of visible irradiation (Fig. 8a-A). Similarly, when pure Fe_2O_3 nonwoven cloth was used as the photocatalyst, the photodegradation of 4-CP was also very slow and only 5.5 % 4-CP was degraded after 120 min (Fig. 8a-B). In addition, with AgBr nonwoven cloth as the photocatalyst, the photodegradation efficiency of 4-CP increased to 52.8 % after 120 min (Fig. 8a-C). Importantly, Fe_2O_3-AgBr nonwoven cloth could degrade 74.2 % 4-CP after 120 min (Fig. 8a-D), also indicating the highest photocatalytic activity of Fe_2O_3-AgBr nonwoven cloth among these nonwoven cloths.

It is well known that mineralization is the ultimate goal in pollutant treatment, and total organic carbon (TOC) value is usually used as an important index for the mineralization degree of organic species. Herein, the mineralization of 4-CP was investigated by immersing 300 mg Fe_2O_3-AgBr nonwoven cloth in 4-CP (100 mL, 20 mg L^{-1}) solution under visible light irradiation (λ> 400 nm), and TOC value was recorded during the photocatalytic process (Fig. 8b). Obviously, with the increase of irradiation time, the TOC concentration continuously decreased, indicating that 4-CP was steadily mineralized. After four hours, the TOC concentration decreases from 12.23 mg L^{-1} to 3.58 mg L^{-1}, reaching a high mineralization ratio of 70.7 %. This fact demonstrates that Fe_2O_3-AgBr nonwoven cloth can efficiently degrade and mineralize organic pollutants under visible light irradiation.

To further confirm the role of the nanojunction in Fe_2O_3-AgBr nonwoven cloth, the degradation efficiencies of RhB and 4-CP were compared (Fig. 9). According to Fig. 7a and 8a, pure Fe_2O_3 nonwoven cloth could degrade 13.7 % RhB after 60 min or 5.5 % 4-CP after 120 min, while pure AgBr nonwoven cloth could degrade 25.9 % RhB after 60 min or 52.8 %

RSC Advances Accepted Manuscript

4-CP after 120 min. Thus, the total degradation efficiencies by two individual photocatalysts (Fe_2O_3 nonwoven cloth and AgBr nonwoven cloth) were 39.6 % (13.7 % + 25.9 %) for RhB after 60 min, or 58.3 % (5.5 % + 52.8 %) for 4-CP after 120 min. More importantly, Fe_2O_3-AgBr nonwoven cloth could degrade 91.8 % RhB after 60 min or 74.2 % % 4-CP after 120 min, which were both higher than the total degradation efficiencies (39.6 % and 58.3 %) by pure Fe_2O_3 nonwoven cloth and pure AgBr nonwoven cloth for RhB and 4-CP degradation. These results strongly reveal that there is a synergic effect in Fe_2O_3-AgBr heterojunction nonwoven cloth, which is similar to the phenomenon in our previous study.[27]

Based on the above results, one can conclude that Fe_2O_3-AgBr nonwoven cloth exhibits higher photocatalytic activity than pure Fe_2O_3 nonwoven cloth and pure AgBr nonwoven cloth with the same weight of each component, even higher than the sum of photocatalytic efficiencies by pure Fe_2O_3 nonwoven cloth and pure AgBr nonwoven cloth, for the photodegradation of RhB and 4-CP. The possible reasons for the highest photocatalytic activity of Fe_2O_3-AgBr nonwoven cloth are analyzed, and we believe that there are chiefly two reasons. One reason is the substantial broadening of the photoabsorption range from the UV to visible-light range, as shown in Fig. 5. Undoubtedly, this broadening facilitates the absorption of more visible light, which produces more photogenerated holes and electrons consequently. The other reason should be due to the energy level matching between Fe_2O_3 and AgBr, as shown in the energy band diagram (Fig. 6b). [38,40] Under the irradiation of visible light, both Fe_2O_3 semiconductor and AgBr semiconductor can generate electrons in the conduction band (CB) and holes in the valence band (VB). As summarized in our recent review,[16] since the CB level of Fe_2O_3 semiconductor is lower than that of AgBr semiconductor, electrons in the CB of AgBr semiconductor can be transferred to that of Fe_2O_3

RSC Advances Accepted Manuscript

semiconductor (Fig. 6b). Furthermore, the VB level of Fe_2O_3 semiconductor is lower than that of AgBr semiconductor, holes in the VB of Fe_2O_3 semiconductor can be transferred to that of AgBr semiconductor (Fig. 6b). As a result, less of a barrier exists due to the promoted separation and migration of photogenerated carriers by the internal field. So the probability of electron-hole recombination can be decreased. Larger numbers of electrons stored on the Fe_2O_3 surface and holes stored on the AgBr surface can, respectively, participate in photoredox reactions to degrade organic pollution directly or indirectly, which can enhance the photocatalytic reaction greatly, just as presented in Fig. 7a and 8a.

Most importantly, the macroscale Fe_2O_3-AgBr nonwoven cloth can be easily transferred and/or recycled in photocatalytic application. To evaluate the stability and reusability of macroscale Fe_2O_3-AgBr nonwoven cloth, a recycling test was performed, as shown in Fig. 10. The photodegradation of RhB was monitored for four cycles (each cycle lasted 60 min). After each cycle, the macroscale Fe_2O_3-AgBr nonwoven cloth was recycled by diping/pulling method and/or external magnetic field, then washed with water. Afterward, the cloth was immersed in the same volume (40 mL) of fresh RhB solution with the same concentration (4.79 mg L^{-1}) again. For the first cycle, 91.8 % RhB was degraded after 60 min reaction time. Subsequently, the degradation efficiency of RhB was 88.6 %, 85.2 % and 79.8 % for the second, third and fourth cycle, respectively (Fig. 10). This fact indicates a slight decrease of degradation efficiency, and the reason for the decrease was further investigated. After 4 times photocatalytic tests, Fe_2O_3-AgBr nonwoven cloth was recycled, and its XRD pattern was also analyzed (Fig. 3a, blue line). Obviously, there is no change of the crystalline phases compared with the as-prepared Fe_2O_3-AgBr nonwoven cloth, which indicates that Fe_2O_3-AgBr nonwoven cloth has excellent stability. In addition, we also found that Fe_2O_3-AgBr nonwoven

RSC Advances Accepted Manuscript

cloth has good stability in the solution with a wide pH range (3-11). For example, when the cloth was immersed in acidic solution (pH= 4.5) for 60 min, the mass loss of Fe_2O_3-AgBr nonwoven cloth was only 4.13 wt%. However, during photocatalytic process, we found that Fe_2O_3-AgBr nonwoven cloth was relatively fragmented, and there was a mass loss from 20 mg for the first cycle to 16.8 mg for the fourth cycle. Thus, the slight decrease of degradation efficiency should be attributed to the mass loss instead of the performance change of Fe_2O_3-AgBr nonwoven cloth. Further work should be carried out to prepare efficient and flexible macroscale Fe_2O_3-AgBr nonwoven cloth with larger area and better mechanical properties.

4. Conclusions

In summary, Fe_2O_3-AgBr nonwoven cloth has been synthesized by a electrospinning-calcination method. Such macroscale cloth consists of nanofibers that were in fact constructed from Fe_2O_3 and AgBr nanoparticles. Under visible light illumination, Fe_2O_3-AgBr nonwoven cloth exhibits excellent photocatalytic activity for the degradation of RhB and 4-CP, compared with nonwoven cloths based on single visible-light response component (pure Fe_2O_3 nonwoven cloth and pure AgBr nonwoven cloth). Furthermore, Fe_2O_3-AgBr nonwoven cloth can be easily transferred and/or recycled with good stability, by diping/pulling method and/or external magnetic field. Therefore, Fe_2O_3-AgBr nonwoven cloth has great potential as efficient and easily recyclable VLD photocatalysts for future practical photocatalytic application, for example, degrading organic pollutants in the polluted river/lake.

RSC Advances Accepted Manuscript

Acknowledgements

This work was financially supported by the National Natural Science Foundation of China (Grant Nos. 21107013, 21377023, and 21477019), Specialized Research Fund for the Doctoral Program of Higher Education (Grant Nos. 20110075120012), the Fundamental Research Funds for the Central Universities, Chinese Universities Scientific Fund (113-06-0019064) for financial support.

Notes and references

a State Environmental Protection Engineering Center for Pollution Treatment and Control in Textile Industry, College of Environmental Science and Engineering, Donghua University, Shanghai 201620, China

b State Key Laboratory for Modification of Chemical Fibers and Polymer Materials, College of Materials Science and Engineering, Donghua University, Shanghai 201620, China

[c] Research Center for Analysis and Measurement, Donghua University, Shanghai 201620, China

1 A. Kubacka, M. Fernandez-Garcia and G. Colon, *Chem. Rev.*, 2012, **112**, 1555-1614.

2 X. B. Chen and S. S. Mao, *Chem. Rev.*, 2007, **107**, 2891-2959.

3 K. Nakata and A. Fujishima, *J. Photoch. Photobio. C.*, 2012, **13**, 169-189.

4 W. C. Huang, L. M. Lyu, Y. C. Yang and M. H. Huang, *J. Am. Chem. Soc.*, 2012, **134**, 1261-1267.

5 G. C. Xi, S. X. Ouyang, P. Li, J. H. Ye, Q. Ma, N. Su, H. Bai and C. Wang, *Angew. Chem. Int. Ed.*, 2012, **51**, 2395-2399.

6 F. Qin, H. P. Zhao, G. F. Li, H. Yang, J. Li, R. M. Wang, Y. L. Liu, J. C. Hu, H. Z. Sun and R. Chen, *Nanoscale*, 2014, **6**, 5402-5409.

7 L. S. Zhang, W. Z. Wang, Z. G. Chen, L. Zhou, H. L. Xu and W. Zhu, *J. Mater. Chem.*, 2007, **17**, 2526-2532.

8 L. S. Zhang, W. Z. Wang, L. Zhou and H. L. Xu, *Small*, 2007, **3**, 1618-1625.

RSC Advances Accepted Manuscript

9 J. Jiang, K. Zhao, X. Y. Xiao and L. Z. Zhang, *J. Am. Chem. Soc.*, 2012, **134**, 4473-4476.

10 Q. Liu, D. Wu, Y. Zhou, H. B. Su, R. Wang, C. F. Zhang, S. C. Yan, M. Xiao and Z. Zou, *ACS Appl. Mater. Inter.*, 2014, **6**, 2356-2361.

11 D. J. Martin, N. Umezawa, X. W. Chen, J. H. Ye and J. W. Tang, *Energ. Environ. Sci.*, 2013, **6**, 3380-3386.

12 N. Z. Bao, L. M. Shen, T. Takata and K. Domen, *Chem. Mater.*, 2008, **20**, 110-117.

13 F. Fang, L. Chen, Y. B. Chen and L. M. Wu, *J. Phys. Chem. C.*, 2010, **114**, 2393-2397.

14 S. B. Yang, Y. J. Gong, J. S. Zhang, L. Zhan, L. L. Ma, Z. Y. Fang, R. Vajtai, X. C. Wang and P.M. Ajayan, *Adv. Mater.*, 2013, **25**, 2452-2456.

15 L. S. Zhang, W. Z. Wang, J. Yang, Z. G. Chen, W. Q. Zhang, L. Zhou and S. W. Liu, *Appl. Catal. A-Gen.*, 2006, **308**, 105-110.

16 H. L. Wang, L. S. Zhang, Z. G Chen, J. Q Hu, S. J. Li, Z. H. Wang, J. S. Liu and X. C. Wang, *Chem. Soc. Rev.*, 2014, **43**, 5234-5244.

17 S. J. Hong, S. Lee, J. S. Jang and J. S. Lee, *Energy Environ. Sci.*, 2011, **4**, 1781-1787.

18 Y. D. Hou, A. B. Laursen, J. S. Zhang, G. G. Zhang, Y. S. Zhu, X. C. Wang, S. Dahl and I. Chorkendorff, *Angew. Chem. Int. Ed.*, 2013, **52**, 3621-3625.

19 H. L. Wang, S. J. Li, L. S. Zhang, Z. G. Chen, J. Q. Hu, R. J. Zou, K. B. Xu, G. S. Song, H. H. Zhao, J. M. Yang, J. S. Liu, *CrystEngComm*, 2013, **15**, 9011-9019.

20 T.W. Kim and K.-S. Choi, *Science*, 2014, **343**, 990-994.

21 Y. Zhou, Q. Zhang, Y. H. Lin, E. Antonova, W. Bensch and G. R. Patzke, *Sci. China Chem.*, 2013, **56**, 435-442.

22 P. Wang, B. B. Huang, X. Y. Qin, X. Y. Zhang, Y. Dai, J. Y. Wei and M. H. Whangbo, *Angew. Chem. Int. Ed.*, 2008, **47**, 7931-7933.

23 Y. P. Bi, H. Y. Hu, S. X. Ouyang, Z. B. Jiao, G. X. Lu and J. H. Ye, *J. Mater. Chem.*, 2012, **22**, 14847-14850.

24 Y. Yu, L. L. Ma, W. Y. Huang, F. P. Du, J. C. Yu, J. G. Yu, J. B. Wang and P. K. Wong, *Carbon*, 2005, **43**, 670-673.

25 Q. Li, B. D. Guo, J. G. Yu, J. R. Ran, B. H. Zhang, H. J. Yan and J. R. Gong, *J. Am. Chem. Soc.*, 2011, **133**, 10878-10884.

26 H. Tada, T. Mitsui, T. Kiyonaga, T. Akita and K. Tanaka, *Nat. Mater.*, 2006, **5**, 782-786.

27 L. S. Zhang, K. H. Wong, Z. G. Chen, J. C. Yu, J. C. Zhao, C. Hu, C. Y. Chan and P. K.

RSC Advances Accepted Manuscript

Wong, *Appl. Catal. A-Gen.*, 2009, **363**, 221-229.

28 L. S. Zhang, K. H. Wong, H. Y. Yip, C. Hu, J. C. Yu, C. Y. Chan and P. K. Wong, *Environ. Sci. Technol.*, 2010, **44**, 1392-1398.

29 D. L. Jiang, S. Q. Zhang and H. J. Zhao, *Environ. Sci. Technol.*, 2007, **41**, 303-308.

30 L. W. Zhang, Y. J. Wang, H. Y. Cheng, W. Q. Yao and Y. F. Zhu, *Adv. Mater.*, 2009, **21**, 1286-1290.

31 M. Kitano, R. Mitsui, D. R. Eddy, Z.M.A. El-Bahy, M. Matsuoka, M. Ueshima and M. Anpo, *Catal. Lett.*, 2007, **119**, 217-221.

32 Z. H. Zhang, L. B. Zhang, M. N. Hedhili, H. N. Zhang, P. Wang, *Nano Lett.*, 2013, **13**, 14-20.

33 J. X. Zhu, Z. Y. Yin, D. Yang, T. Sun, H. Yu, H. E. Hoster, H. H. Hng, H. Zhang and Q. Y. Yan, *Energy Environ. Sci.*, 2013, **6**, 987-993.

34 J. Sundaramurthy, P. S. Kumar, M. Kalaivani, V. Thavasi, S.G. Mhaisalkar and S. Ramakrishna, *RSC Adv.*, 2012, **2**, 8201-8208.

35 Y. D. Guo, G. K. Zhang, J. Liu and Y. L. Zhang, *RSC Adv.*, 2013, **3**, 2963-2970.

36 J. F. Guo, B. W. Ma, A. Y. Yin, K. N. Fan and W. L. Dai, *Appl. Catal. B-Environ.*, 2011, **101**, 580-586.

37 S. J. Li, L. S. Zhang, H. L. Wang, Z. G. Chen, J. Q. Hu, K. B. Xu and J. S. Liu, *Sci. Rep.*, 2014, **4**, 3978.

38 P. Wang, B. B. Huang, Y. Dai and M. H. Whangbo, *Phys. Chem. Chem. Phys.*, 2012, **14**, 9813-9825.

39 Y. Hou, X. Y. Li, Q. D. Zhao, G. H. Chen and C. L. Raston, *Environ. Sci. Technol.*, 2012, **46**, 4042-4050.

40 Y. Xu and M. A.A. Schoonen, *Am. Mineral.*, 2000, **85**, 543-556.

RSC Advances Accepted Manuscript

Figure Captions:

Fig. 1. Schematic illustration of the preparation of Fe_2O_3-AgBr nonwoven cloth.

Fig. 2. The photos and microscopy images of nonwoven cloth: (a-c) as-prepared PVP/Fe_2O_3-AgBr/CTAB composite nonwoven cloth, (d-f) Fe_2O_3-AgBr nonwoven cloth, (g-h) TEM images of one nanofiber from Fe_2O_3-AgBr nonwoven cloth.

Fig. 3. (a) XRD patterns of the as-prepared Fe_2O_3-AgBr nonwoven cloth, the used Fe_2O_3-AgBr nonwoven cloth after photocatalytic test, and the standard patterns of AgBr (JCPDS Card. 79-0149) and Fe_2O_3 (JCPDS Card. 87-1166), and (b) EDS pattern of Fe_2O_3-AgBr nonwoven cloth.

Fig. 4. (a) Magnetic hysteresis loops of Fe_2O_3-AgBr nonwoven cloth, a detailed partial image is shown in the inset of the figure, and magnetic separation test of Fe_2O_3-AgBr nonwoven cloth: (b) without the external magnet field, and (c) with the external magnet field.

Fig. 5. The ultraviolet-visible diffuse reflectance spectra of Fe_2O_3 cloth and Fe_2O_3-AgBr cloth.

Fig. 6. (a) Schematic illustration of experimental setups and photocatalytic process, and (b) energy band diagram of the Fe_2O_3-AgBr nonwoven cloth.

Fig. 7. (a) The degradation efficiency of RhB (4.79 mg L^{-1}, 40 mL) by blank test (without photocatalyst), pure Fe_2O_3 nonwoven cloth (11.4 mg), pure AgBr nonwoven cloth (8.6 mg), or Fe_2O_3-AgBr nonwoven cloth (20 mg, containing 11.4 mg Fe_2O_3 and 8.6 mg AgBr), and (b) the effect of pH on the photodegradation efficiency of RhB (4.79 mg L^{-1}, 40 mL) by Fe_2O_3-AgBr nonwoven cloth (20 mg) after 60 min reaction.

Fig. 8. (a) The degradation efficiency of 4-CP (10 mg L^{-1}, 50 mL) by blank test (without

RSC Advances Accepted Manuscript

503 photocatalysts), pure Fe_2O_3 nonwoven cloth (28.5 mg), pure AgBr nonwoven cloth (21.5 mg),
504 or Fe_2O_3-AgBr nonwoven cloth (50 mg, containing 28.5 mg Fe_2O_3 and 21.5 mg AgBr), and (b)
505 the TOC removal efficiency during the 4-CP (20 mg L^{-1}, 100 mL) photodegradation process
506 by Fe_2O_3-AgBr nonwoven cloth (300 mg).
507 **Fig. 9.** The comparison of degradation efficiencies of RhB after 60 min and 4-CP after 120
508 min, by Fe_2O_3 nonwoven cloth, AgBr nonwoven cloth and Fe_2O_3-AgBr nonwoven cloth.
509 **Fig. 10.** Cycling photocatalytic test of Fe_2O_3-AgBr nonwoven cloth (20 mg).
510
511
512
513
514
515
516
517
518
519
520
521
522
523
524
525
526
527

RSC Advances Accepted Manuscript

Figures

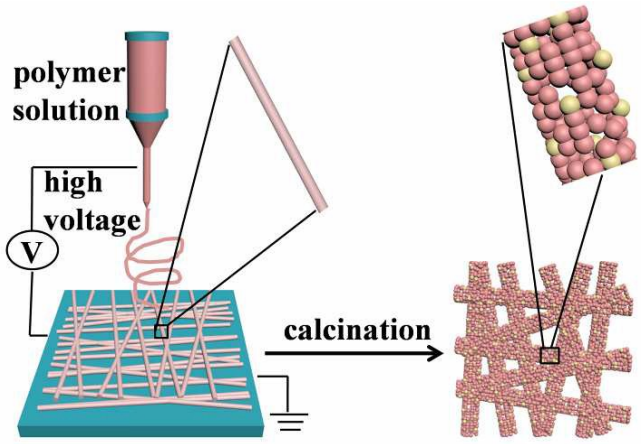

Fig. 1.

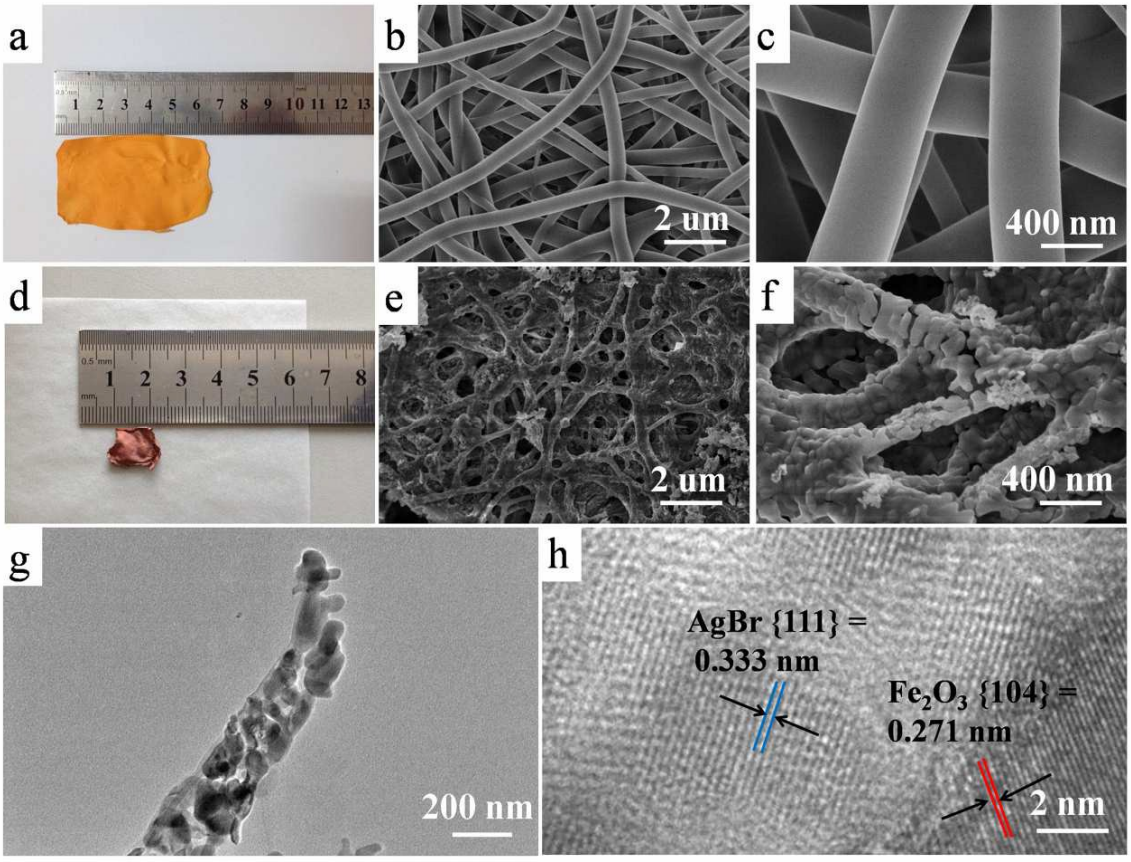

Fig. 2.

RSC Advances Accepted Manuscript

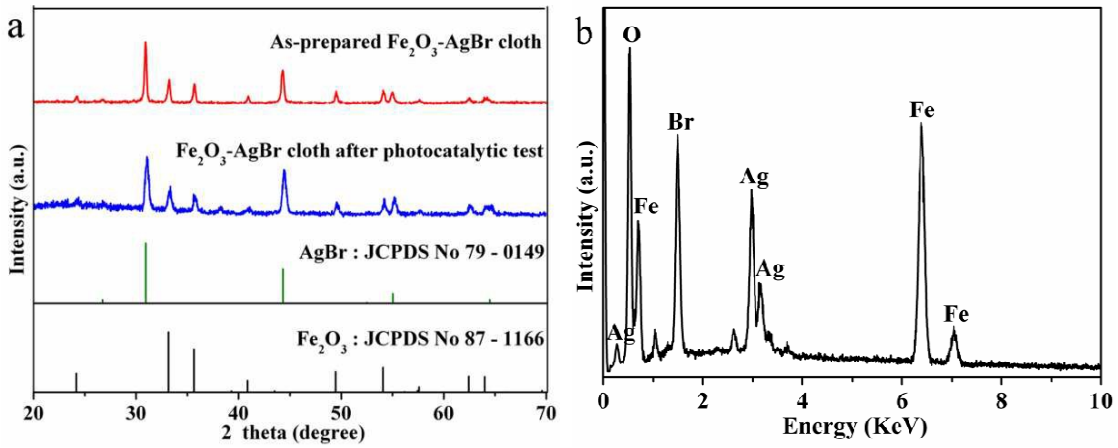

537

538 **Fig. 3.**

539

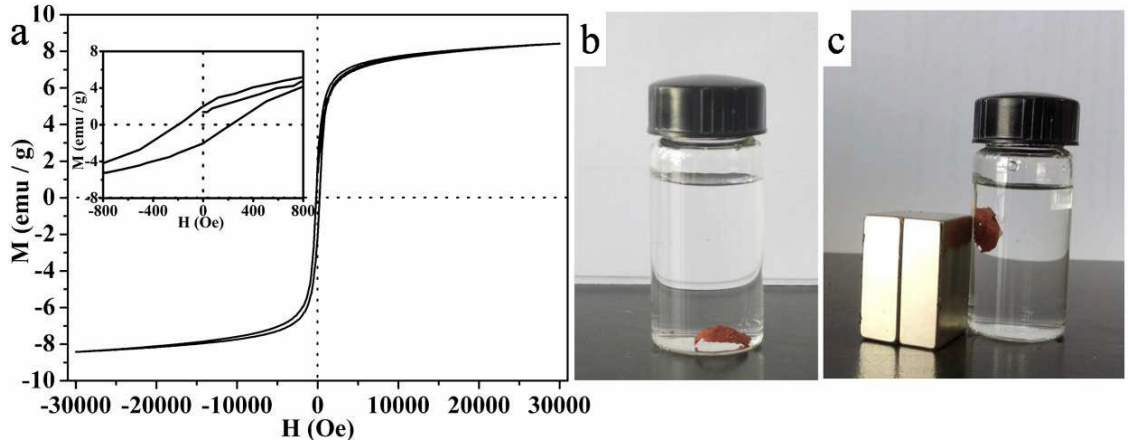

540

541 **Fig. 4.**

542

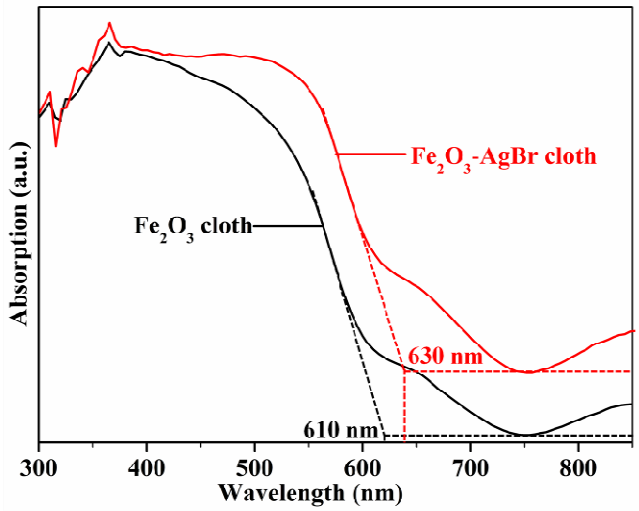

543

544 **Fig. 5.**

RSC Advances Accepted Manuscript

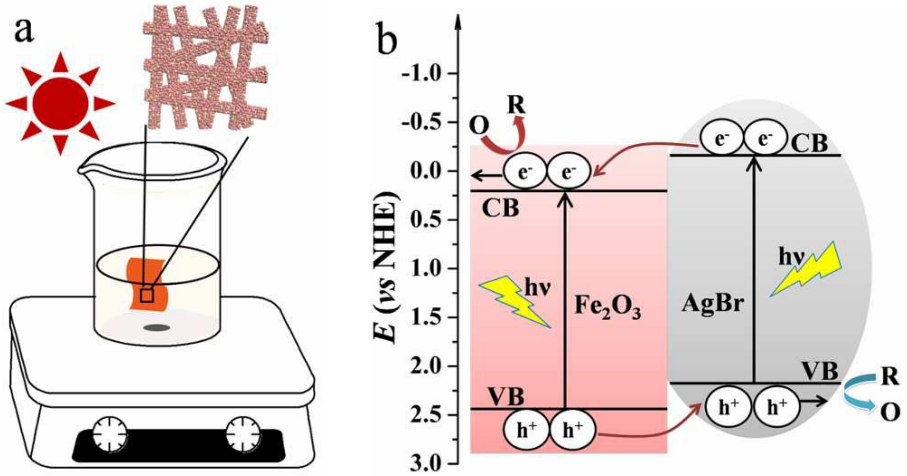

Fig. 6.

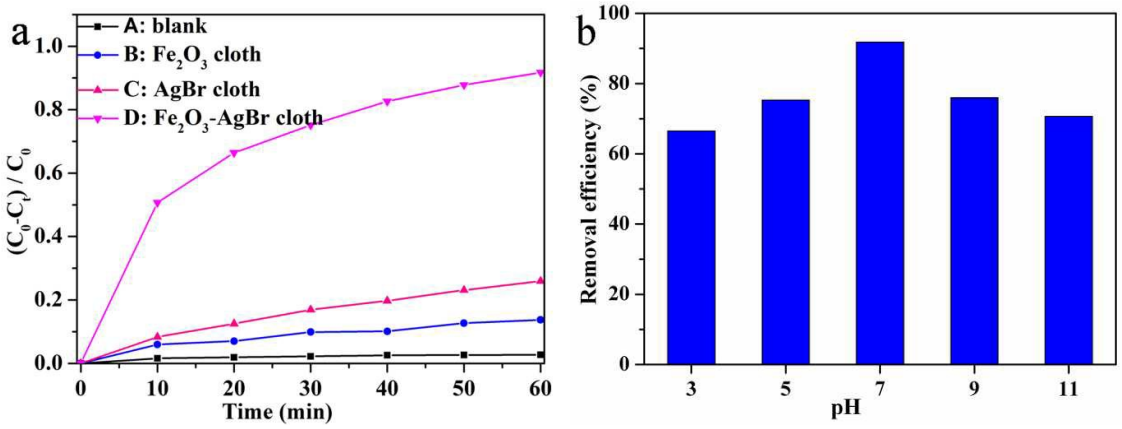

Fig. 7.

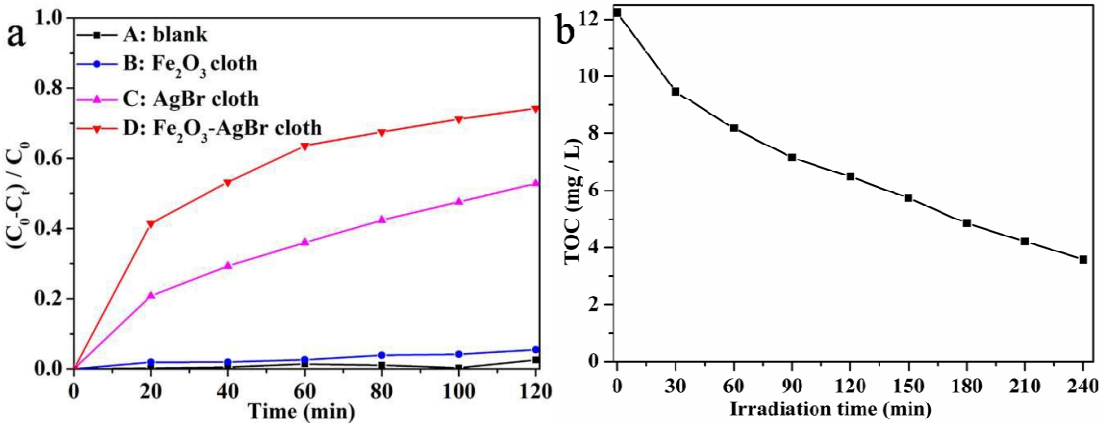

Fig. 8.

RSC Advances Accepted Manuscript

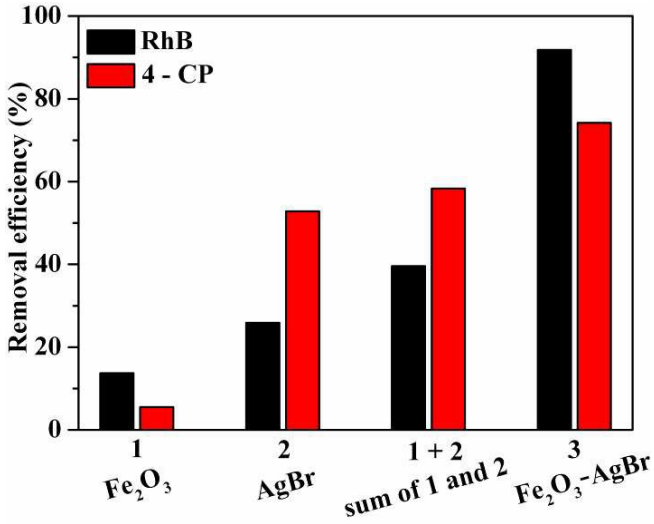

Fig. 9.

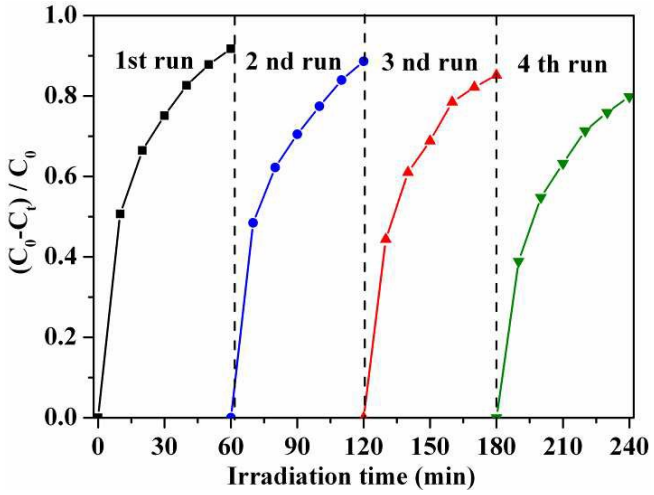

Fig. 10.

RSC Advances Accepted Manuscript